

Phosphorescence

Zitierweise: *Angew. Chem. Int. Ed.* **2022**, *61*, e202111805

Internationale Ausgabe: doi.org/10.1002/anie.202111805

Deutsche Ausgabe: doi.org/10.1002/ange.202111805

Mapping the Regioisomeric Space and Visible Color Range of Purely Organic Dual Emitters with Ultralong Phosphorescence Components: From Violet to Red Towards Pure White Light

Bibhisan Roy, Iván Maisuls, Jianyu Zhang, Felix C. Niemeyer, Fabio Rizzo, Christoph Wölper, Constantin G. Daniliuc, Ben Zhong Tang,* Cristian A. Strassert* and Jens Voskuhl*

Abstract: We mapped the entire visible range of the electromagnetic spectrum and achieved white light emission (CIE: 0.31, 0.34) by combining the intrinsic ns-fluorescence with ultralong ms-phosphorescence from purely organic dual emitters. We realized small molecular materials showing high photoluminescence quantum yields (Φ_L) in the solid state at room temperature, achieved by active exploration of the regioisomeric substitution space. Chromophore stacking-supported stabilization of triplet excitons with assistance from enhanced intersystem crossing channels in the crystalline state played the primary role for the ultra-long phosphorescence. This strategy covers the entire visible spectrum, based on organic phosphorescent emitters with versatile regioisomeric substitution patterns, and provides a single molecular source of white light with long lifetime (up to 163.5 ms) for the phosphorescent component, and high overall photoluminescence quantum yields (up to $\Phi_L = 20\%$).

Introduction

Isomerism is an important design concept that has remarkable consequences on the physical and chemical properties of molecular entities. It is well known that stereoisomers show notably divergent pharmacokinetic profiles and pharmacodynamic properties, depending on their intrinsic chiral information.^[1] For instance, this is the case for the common pain reliever Ibuprofen, where the S+ isomer is the pharmacologically active form, whereas the R- enantio-

mer has no anti-inflammatory effect.^[2] On the other hand, regioisomerism often alters the properties of materials.^[3] By definition, regioisomers are constitutional isomers that have the same functional groups attached at different positions of the molecular backbone. Due to distinct positioning of these groups, regioisomerism has a dramatic impact on the energy levels (both singlet and triplet) of a chromophoric entity.^[4] Taking this effect into account, much effort has already been invested with the aim to develop smart luminescent and photovoltaic materials.^[4a-c] However, up to date and to the best of our knowledge, a similar kind of attempt has not been undertaken to tune the triplet state energy in order to alter the phosphorescence of dual emitters with the objective of covering the whole visible spectrum.

It is widely known that phosphorescence arises from the usually spin-forbidden radiative decay from the lowest excited triplet state (T_1) to the singlet ground state (S_0). Therefore, efficient phosphorescence depends on the ability of a molecule to competitively undergo a non-radiative transition from the S_1 to T_1 state via vibration-triggered intersystem crossing (ISC).^[5] Besides that, the relative efficiency of ISC further depends on the energy gap between the lowest excited singlet and the involved triplet state (ΔE_{ST}) as well as on the spin orbit coupling (SOC) strength.^[5d,e,6] Notably, efficient SOC can be facilitated by the presence of heavy elements, most prominently late transition metals.^[7] Thereby, most of the phosphorescent materials developed so far contain scarce metal centers, such as Re, Ru, Os, Rh, Ir,

[*] Dr. B. Roy, Dr. F. C. Niemeyer, Jun.-Prof. Dr. J. Voskuhl
Faculty of Chemistry (Organic Chemistry) and Center for Nano-Integration (CENIDE), University of Duisburg-Essen
Universitätsstrasse 7, 45117 Essen (Germany)
E-Mail: jens.voskuhl@uni-due.de


Dr. I. Maisuls, Prof. Dr. C. A. Strassert
Institut für Anorganische und Analytische Chemie, CeNTech, CiMIC, SoN, Westfälische Wilhelms-Universität Münster
Heisenbergstraße 11, 48149, Münster (Germany)
E-Mail: cstra_01@uni-muenster.de


J. Zhang, Prof. Dr. B. Z. Tang
Department of Chemistry, Hong Kong University of Science and Technology (HKUST)
Clear water Bay, Kowloon (Hong Kong)
E-Mail: tangbenz@ust.hk

Dr. F. Rizzo, Dr. C. G. Daniliuc
Organisch Chemisches Institut, Westfälische Wilhelms-Universität Münster (F.R. and C.G.D.) and SoN (F.R.)
Corrensstraße 36, 48149 Münster (Germany)

Dr. C. Wölper
Institute for Inorganic Chemistry and Center for NanoIntegration (CENIDE), University of Duisburg-Essen
Universitätsstrasse 5-7, 45117 Essen (Germany)

Dr. F. Rizzo
Institute of Chemical Science and Technologies „G. Natta“ (SCITEC), National Research Council (CNR)
Via G. Fantoli 16/15, 20138 Milan (Italy)

 Supporting information and the ORCID identification number(s) for the author(s) of this article can be found under:
<https://doi.org/10.1002/anie.202111805>

 © 2021 The Authors. Angewandte Chemie published by Wiley-VCH GmbH. This is an open access article under the terms of the Creative Commons Attribution Non-Commercial License, which permits use, distribution and reproduction in any medium, provided the original work is properly cited and is not used for commercial purposes.

Pd, Pt and Au, among others.^[8] Such phosphorescent metal complexes received attention in the frame of chemosensing,^[8b] bioimaging and optoelectronics, although their high costs as well as their quenching sensitivity towards triplet molecular dioxygen limits their scope. In contrast, organic phosphorescent materials (OPM) are often easily accessible and hence they are currently receiving growing attention.^[9] However, the practical development of OPM is a challenging task owing to the inefficient SOC observed in pure organic molecules.^[5c,10] As known, weak SOC of organic molecules cannot provide the ability to afford efficient ISC to create triplet excitons. Simultaneously, due to the fact that the radiative deactivation (phosphorescence) is usually spin-forbidden in the absence of relativistic SOC-related mixing of spin-states (which is typically promoted by late transition elements), other non-radiative decay pathways (such as vibrational relaxation and ³O₂-mediated quenching, among others) causes the radiationless loss and thermalization of triplet excitons.^[5c] Hence, an intelligent design of efficient OPM requires a significant improvement of the ISC efficiency by increasing the density of states in the triplet manifold (as stated in Fermi's golden rule) along with a suppression of detrimentally competitive non-radiative decays. One way to improve the ISC of organic probes is by the introduction of halogens, carbonyl or sulfone-like functional groups bearing non-bonding electron pairs that provide energetically close-lying states with different spin multiplicities and orbital angular momenta, thus facilitating ISC, according to El Sayed's rule.^[5c,10a,11] In addition, non-radiative decay pathways can be significantly reduced upon aggregation of molecules in the solid or crystalline state, due to a shielding from molecular oxygen and locking of rotovibrational modes.^[12]

Hence, as long as intermolecular quenching phenomena are suppressed, aggregation also enhances molecular stacking by bringing the chromophores in closer contact.^[13] Such arrangement plays a significant role to enhance the excited state and phosphorescence lifetimes.^[5d] By controlling the chromophore stacking in the solid state, it is also possible to tune the overall photoluminescence color as well as the phosphorescence afterglow. In this context, regioisomerism can be the right choice to precisely tune the stacking of chromophores upon variation of the functional groups' position, without changing the molecular formula. Purely organic triplet emitters with tunable lifetimes and diverse colors are of high importance and can be used in various applications, such as data encryption,^[14] anti-counterfeiting^[15] and biological imaging,^[16] among many others.^[17] Here, we present a strategy to employ this concept enabling a full-range color tuning towards white light emission based on dual emitters with ultra-long phosphorescence.

It is noteworthy that the realization of single-sourced white light emitters still remains a challenging task, especially if aiming at small molecule-based materials. Typically, single source white light emission (SSWLE) requires multicomponent systems, since white light emission (WLE) needs simultaneous luminescence of the three primary (red, green, and blue, i.e., RGB)^[19] or at least two complementary (yellow and blue, i.e., YB) colors.^[20] Hence, SSWLE is difficult to

achieve due to their specific requirements of different emission wavelengths (RGB/YB). Tang et al. reported on a chlorinated dibenzothiophene derivative, featuring white-light emission with moderate quantum yields ($\Phi_L = 7.2\%$) and long lifetimes of 123.4 ms.^[20a] Very recently, Chi and co-workers reported the use of dibenzofuran (DBF), which was reacted with benzenesulfonyl chloride yielding two compounds, featuring long lifetimes and tunable emission wavelength, which were also investigated in depth in our present study for benchmarking our new luminophores (Table 1).^[18] Cao and co-workers also recently reported an isomeric 9-phenyl-9H-carbazole (PhCz) donor-acceptor system featuring dual emission properties (fluorescence and phosphorescence), leading to pure white light emission (CIE = 0.33, 0.34). Additionally, they achieved efficient recognition of fingerprints with these compounds.^[21] In this pioneering work, white light emission as well as first indication of the role of regioisomerism was observed, but not systematically explored. Although numerous other white light emitters have been described in literature,^[22] none of these previous works achieved our high quantum yields, broad lifetime ranges and full color tunability over the whole visible part of the electromagnetic spectrum towards white light emission. Color tuning has been achieved according to literature reports using thermally activated delayed fluorescence (TADF)^[23] or fluorescence^[24] approaches, whereas the implementation of

Table 1: Phosphorescence lifetime components (τ) with their relative amplitudes and steady-state (global, that is, fluorescence + phosphorescence) photoluminescence quantum yields (Φ_L) of all twelve isomers in the crystalline state.^[a]

Sample	τ [ms] ($\lambda_{em} \approx 550$ nm)	Φ_L ($\pm 2\%$)
1-PhDBF ^[a]	$\tau_1 = 132 \pm 4$ (48%), $\tau_2 = 20 \pm 3$ (52%), $\tau_{av} = 74 \pm 3$	15
2-PhDBF	$\tau_1 = 77 \pm 4$ (26%), $\tau_2 = 9.7 \pm 0.6$ (74%), $\tau_{av} = 27 \pm 1$	22
3-PhDBF ^[a]	$\tau_1 = 141 \pm 12$ (46%), $\tau_2 = 18 \pm 3$ (54%) $\tau_{av} = 75 \pm 5$	12
1-PhClDBF	$\tau_1 = 57 \pm 3$ (30%), $\tau_2 = 10 \pm 1$ (70%), $\tau_{av} = 24 \pm 1$	12
2-PhClDBF	$\tau_1 = 300 \pm 16$ (42%), $\tau_2 = 42 \pm 4$ (58%) $\tau_{av} = 150 \pm 6$	19
3-PhClDBF	$\tau_1 = 160 \pm 8$ (35%), $\tau_2 = 25 \pm 2$ (65%), $\tau_{av} = 72 \pm 2$	18
1-PhBrDBF	$\tau_1 = 79 \pm 6$ (36%), $\tau_2 = 15.0 \pm 1.5$ (64%), $\tau_{av} = 38 \pm 2$	7
2-PhBrDBF	$\tau_1 = 271 \pm 11$ (54%), $\tau_2 = 37 \pm 5$ (46%), $\tau_{av} = 164 \pm 6$	20
3-PhBrDBF	$\tau_1 = 136 \pm 5$ (54%), $\tau_2 = 24 \pm 2$ (46%), $\tau_{av} = 84 \pm 2$	16
1-PhIDBF	$\tau_1 = 84 \pm 3$ (7%), $\tau_2 = 22 \pm 1$ (38%), $\tau_3 = 4.6 \pm 0.3$ (55%), $\tau_{av} = 16.4 \pm 0.3$	8
2-PhIDBF	$\tau_1 = 52 \pm 3$ (7%), $\tau_2 = 17.0 \pm 1.3$ (50%) $\tau_3 = 5.5 \pm 0.6$ (43%), $\tau_{av} = 14.00 \pm 0.15$	2
3-PhIDBF	$\tau_1 = 131 \pm 9$ (11%), $\tau_2 = 34 \pm 4$ (38%), $\tau_3 = 9 \pm 1$ (51%), $\tau_{av} = 31.2 \pm 0.6$	4

[a] The time-resolved photoluminescence decays, including the individual fitting components and confidence limits can be seen in the Supporting Information, Figures S87–S110). τ_{av} = amplitude-weighted average lifetime.^[a] The photophysical properties have been reported in parts beforehand.^[18]

phosphorescence for this purpose has not been explored yet, to the best of our knowledge. By carefully tuning the S_1 and T_1 states, we now aimed for an in-depth investigation of the influence of regioisomerism on the luminescence and white-light emission properties, an aspect that has not been considered so far. In particular, we investigated the influence of halogenated and non-halogenated sulfones attached at three different positions on DBF, focusing on the emission wavelength, excited state lifetimes as well as photoluminescence quantum yields (Φ_L). To this end, a library of twelve compounds was synthesized and studied in detail, including 4 sets of compounds, each consisting of 3 regioisomers equipped with halogenated and non-halogenated benzenesulfones. Two of the compounds, namely 1- and 3-PhDBF, were reported in the literature almost simultaneously to our present study and were used herein for comparative benchmarking.^[18]

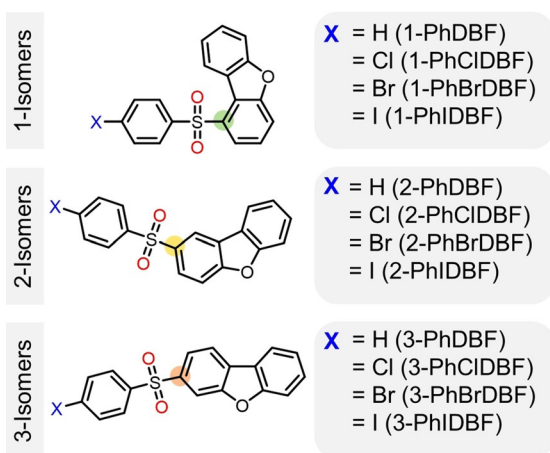
The designed systems achieved color tunability over the whole visible spectrum, while reaching single source white light emission (SSWLE) in the solid state at room temperature. This goal has been reached by tuning the triplet energy through chromophore stacking. The synthesis of the library was carried out using DBF as the electron-rich part of the chromophore, which we synthesized ourselves^[25] to circumvent the ongoing debate on impurities in commercially available compounds for the design of phosphorescence emitters (Figure S1).^[4b] This DBF was coupled in a Friedel–Crafts-like reaction with (halogenated) benzenesulfonylchlorides using aluminum(III) chloride as a catalyst.^[26] The sulfone moiety was expected to act as the electron-poor group with additional n -electrons for the availability of excited n - π^* configurations, whereas both aromatic rings can be regarded as contributing to the π - π^* -character (which are both required to promote ISC, according to El Sayed's rule).^[27] Since DBF contains several positions for the reaction with the sulfonylchlorides, we were able to isolate three different isomers from each reaction batch, which were successfully characterized and crystallized in their pure forms, yielding a library of twelve different DBF-based emitters in total (see Scheme 1, S1, S2 and Figures S2–S52), while featuring halogenated and non-halogenated benzenesulfones to further

tune the ISC rates. Additionally, all compounds were obtained as single crystals suitable for X-ray diffractometric analysis (Figures S113–S127 and Table S4–S7).^[28] Fascinatingly, all the designed isomers showed ultralong phosphorescence lifetimes (>10 ms) along with high Φ_L in the crystalline state (Table 1 and Supporting Information, Movie S1–S4).

Notably, the observed ultra-long phosphorescence of the non-halogenated isomers (PhDBF series, $X = H$, Scheme 1), which have been reported in parts (1- and 3-PhDBF) beforehand,^[18] demonstrated that the halogen substitution is not strictly necessary for the phosphorescence at room temperature. However, the positional alterations of the regioisomers were found to be extremely important to tune the triplet state energy by modulation of the chromophore (DBF-DBF) stacking. This ultimately results in a broad range of phosphorescence colors. With all twelve isomers in hand, we were able to achieve an unprecedented full-color emission range (from violet to red) and even SSWLE (Commission Internationale de l'éclairage, that is, CIE, 0.29, 0.35 for 2-PhBrDBF and 0.31, 0.34 for 3-PhBrDBF, for further information see Supporting Information), while featuring notably high photoluminescence quantum yields (up to 20%) and ultralong phosphorescence lifetimes (up to 164 ms, see Table 1). To the best of our knowledge, this is one of the first systematic reports of regioisomerism-controlled ultralong phosphorescence with full color tunable emission range in the visible range as well as efficient SSWLE. We anticipate that this combined synthetic, spectroscopic and theoretical work will provide an important platform to design the next generation of multi-color emitters with ultralong lifetimes, without the need for scarce transition metal elements.

Results and Discussion

Initially, the optical properties of each isomer were assessed in fluid solutions at RT. All isomers revealed nearly unaltered dual UV/Vis absorption bands (maxima at ca. 290 nm and weak shoulders at 310 nm, for example, in acetonitrile) independently of the solvent polarity (Figure S53). The observed high energy absorption bands are therefore attributed to the transition into π - π^* -configured states and the low-energy band are assigned to absorptive processes into intramolecular charge-transfer states (ICT with n - π^* character) from the DBF moiety to the benzenesulfone group. Furthermore, theoretical calculations showed that the highest occupied molecular orbital (HOMO) and lowest unoccupied molecular orbital (LUMO) mainly reside on the DBF and the benzenesulfone moieties, respectively (Figures S55, S56). This observation confirms the assumption that ICT from the electron rich DBF (donor) to electron poorer benzenesulfone (acceptor) moiety can occur. Moreover, the emission maxima of each isomer were also found to gradually red shift upon enhancing the polarity of solvents (Figure S57), which finally confirm our assignment to a characteristic ICT state. In addition, the short photoluminescence components in THF solution (in the order of ns) strongly suggest



Scheme 1. Chemical formulae of the investigated regioisomers.

fluorescence emission from the excited singlet state (Figures S58–S70, Table S1).

To investigate the optical properties of the molecules in their crystalline form, which were grown for all twelve compounds, the photoluminescence spectra using different delays (0, 5, 10 and 50 μ s) were measured (Figures S75–S86, Table S2). Without delay, the observed spectra showed vibrationally unstructured dual emission bands for all isomers (see Figure S54 for the excitation spectra of the crystals, which were used for the selection of the excitation wavelengths): Mainly a high-energy band in the blue region (ca. 400 nm to 450 nm) and a low-energy band in the greenish/yellow range (ca. 500 nm to 580 nm) were detectable (Figures S71–S74, $\lambda_{\text{ex}} = 376.7$ nm). This dual emission is explained by the donor-acceptor nature (D-A, namely, push-pull character) of the luminophores (see above). Upon excitation, the availability of D-A excited singlet states lead to a high-energy (ca. 400 nm to 450 nm) fluorescence band and a pronounced lower-lying phosphorescence shoulder (ca. 500 nm to 580 nm) involving the electron-rich DBF donor and the electron poorer benzosulfone acceptor. The intensity of both bands were found to vary between the different regioisomers, as observed in Figures S71–S74, which mirrors the different relative ISC rates, radiative and radiationless deactivation rates involving the singlet and triplet manifolds. These phenomena can be also affected by the various conformations and the relative twisting of the moieties caused by the packing differences in the crystalline state (Figure S134–S139). As a representative example, 1-PhDBF exhibits the blue peak as a weaker band (ca. 430 nm) and an intense phosphorescence shoulder (ca. 530 nm), but in the case of 2-PhDBF, the relative intensities appear reversed (Figures S71).

Time-gated emission spectra were also measured with different delay times in order to explore the slow radiative relaxation pathways, that is, phosphorescence (Figures S75–S86), where the short-lived fluorescence will be mostly depleted (Figure S148). After 5 μ s of delay, the photoluminescence (PL) emission spectra display two unstructured emission bands almost for all isomers. In general, a peak at higher energy (ca. 400 nm to 450 nm) and an intense band at lower energy (ca. 500 nm to 650 nm) were observed (Figures S75–S86). Interestingly, the intensity of the high-energy peak was gradually attenuated upon increasing the delay time to 10 μ s, and ultimately completely disappeared at 50 μ s delay; hence, only a single band at lower energies (ca. 500 nm to 650 nm) remained for all isomers and can be clearly assigned to the phosphorescence from ICT triplet states. For further confirmation of our assumption, we pursued excited state photoluminescence lifetime measurements of all the isomers, as depicted in Table 1. Fascinatingly, the lifetime values of the lower energy emission bands (ca. 500 nm to 650 nm) are in the order of the ms for all the evaluated isomers (Figures S87–S110), where the shortest amplitude-weighted average lifetime ($\tau_{\text{av-amp}}$) was found at 14 ms (2-PhIDBF) and the longest one reached 164 ms (2-PhBrDBF), see Table 1. This ultra-long decay confirms that the low-energy band is associated with room-temperature phosphorescence. It has been previously reported that the emission in the solid state depends on the photophysics of individual

molecules as well as on non-covalent interactions between the molecules.^[29] It should be noted that numerous intermolecular non-covalent interactions within the crystal lattice can facilitate the formation of different kinds of aggregates, experiencing distinct environments. Therefore, multiexponential lifetimes can be observed, as it is in the present case (Table 1).

Notably, the phosphorescence of each isomer can be also directly visualized by naked eye up to two seconds after turning off the photoexcitation source (Figure 1 and supporting information) going along with a progressive change in the afterglow color. This unique observation could grant advantages in many technological areas, like information encryption and anti-counterfeiting applications, among others.^[14–15,17] Moreover, time-resolved photoluminescence decay analysis of the lower-energy band provided noteworthy trends within a set of regioisomers (Table 1). As observed, apart from the iodine-substituted species, all other isomers exhibit a bi-exponential decay profile. The bi-exponential decay of these crystals suggests, as mentioned above, at least two distinct microenvironments sensed by the luminophores within the crystal (for example, a herringbone packing, see below). After careful examination of the lifetimes, it was noticed that the shortest values among all the isomer families correspond to the iodine-substituted compounds (14 ms to 31 ms, Table 1, Figures S106, S108 and S110). This outcome can be attributed to the non-radiative decay facilitated by the weaker-bonded iodine moiety along with the heavy atom related higher SOC promoting the spin-forbidden ISC process ($T_1 \rightarrow S_0$, see below). On the other hand, 2-PhCIDBF and 2-PhBrDBF showed the longest phosphorescence lifetimes (150 ms and 164 ms, respectively) whereas 1-PhCIDBF and 1-PhBrDBF showed the shortest values (24 ms and 38 ms, respectively) in these series (Table 1, Figures S94, S96, S100, and S102). The longest values observed for the 2-isomers can be explained by the chromophore stacking mode (Figure 3), whereas the 1-isomers reveal a lack of such interactions in the crystal, as explained in the next paragraphs. Another interesting observation is the appearance of long amplitude-weighted average lifetimes (27 ms to 74 ms) for the unsubstituted compounds, which has been reported in parts beforehand (PhDBF series) (Table 1, Figures S87–S92).^[18] This result demonstrates that the halogen substituents are not essential to induce phosphorescent afterglow. It should be highlighted that triplet emitters based on pure organic molecules with ultralong lifetimes (> 10 ms) are very scarce and in most cases considered as an isolated and peculiar event. Therefore, these organic phosphorescence emitters will surely enrich the palette of luminophores in this field.

One of the most notable observations of this work is the progression of the afterglow color upon pulsed UV excitation (365 nm) featured by the crystalline samples of selected regioisomers (see Figure 2A). Impressively, the twelve regioisomers can cover the whole visible range of the electromagnetic spectrum.

Under steady-state excitation, white light emission can be also achieved (Figure 2B–D). In this regard, these properties were the outcome of the energetic tuneability affecting both triplet and singlet states and supported by the positional

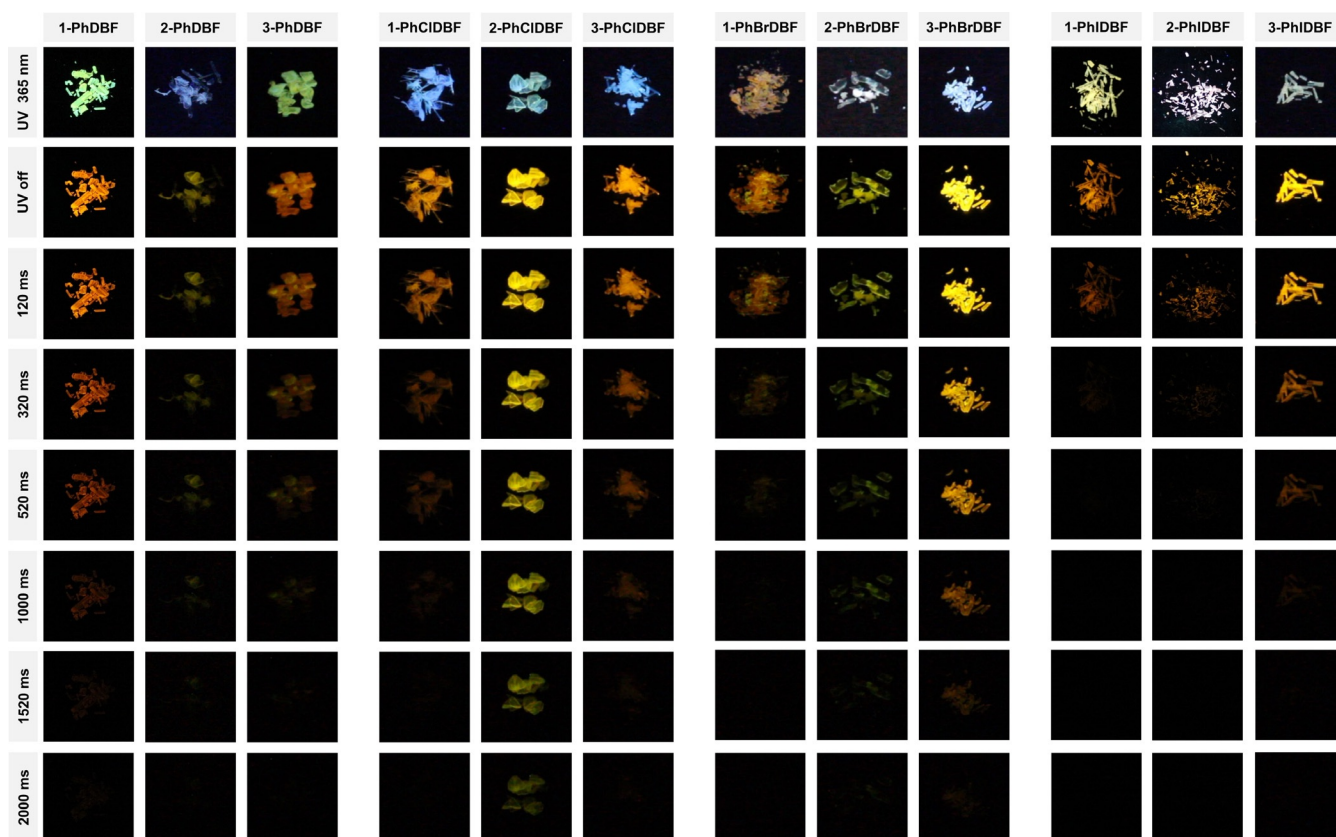


Figure 1. Persistent phosphorescence (after UV excitation is turned off) and prompt emission (under 365 nm UV light, during irradiation with a hand-lamp) of all regioisomers as crystalline solids at room temperature (qualitative experiment, the actual lifetimes can be found in Table 1). The phosphorescence afterglow can be seen up to 2 s by naked eye upon interruption of the photoexcitation. Note: the delay times depicted should be regarded as ± 40 ms, due to the experimental uncertainty, see Supporting Information for details. Parts of the characterization of 1-PhDBF and 3-PhDBF has been reported beforehand.^[18]

isomerization, as will be shown in the subsequent paragraphs. As a representative example of the combination of singlet and triplet emission, the PhDBF isomers reveal blue to green luminescence under steady-state excitation with UV-light (Figure 1, Figures S71, Table S2). However, after turning off UV light, an orange ($\lambda_{em} = 609$ nm, 1-PhDBF), a greenish-yellow ($\lambda_{em} = 555$ nm, 2-PhDBF) or an red-orange ($\lambda_{em} = 612$ nm, 3-PhDBF) phosphorescent afterglow were observed (Figure 1, Figures S75–S77, Table S2). For the halogen-substituted isomers, similar observations can be documented, but with higher energies during steady-state irradiation and lower energies upon switch-off of the light source (Figures S78–S86, Table S2; for a brief discussion on the influence of substitution patterns and halogens, see Note S2 and Table S3 in the Supporting Information). Most notably, the bromo-substituted isomers, namely 2-PhBrDBF and 3-PhBrDBF, exhibit SSWLE (CIE: 0.29, 0.35 and 0.31, 0.34) under steady-state excitation at 350 nm (Figures 2C and D, S111, S112). In the present case, both isomers show SSWLE as an outcome of the complementary yellow and blue emission (Figures 2C, D). Strikingly, both SSWLE phenomena reveal high overall ϕ_L (20% and 16%) and long $\tau_{av,amp}$ (164 ms and 84 ms, Figures S102 and S104, Table 1). Up to date and to the best of our knowledge, this is the first report of dual-emission-based SSWLE uniting both long lifetimes and high quantum yields.

Since all compounds were obtained as high-quality single crystals, we investigated the packing for all regioisomers. Such high-quality crystals of the first, second and third series of isomers were grown using DCM/MeOH, chlorobenzene/MeOH and cyclohexane/DCM as 1:1 mixtures, respectively (see Supporting Information for details). These crystals were also used for the full photophysical characterization, including the global phosphorescence quantum yields and phosphorescence lifetimes discussed above. Each isomer exhibits numerous non-covalent interactions (Figures S125–S131) that generate a rigid environment leading to a suppression of molecular vibrations, which account for the high quantum yields and long lifetimes. The most important interactions were found to be C–H $\cdots\pi$ and $\pi\cdots\pi$ contacts as analyzed with Hirshfeld analysis (Crystal Explorer,^[30] see Supporting Information), which can influence Φ_L drastically. Notably, Φ_L appeared to follow the proportional relationship of the C–H $\cdots\pi$ to $\pi\cdots\pi$ interactions ratio (ρ) (Table S8).^[31] Here, it is worth to mention that the $\pi\cdots\pi$ stacking is important to stabilize the triplet state, whereas C–H $\cdots\pi$ interactions are important for the restriction of intramolecular motion (RIM). For example, in the series of PhBrDBF, the isomers follow the trend for (ρ): 2-PhBrDBF (4.96) > 3-PhBrDBF (3.36) > 1-PhBrDBF (2.49) that correlates with the increase in the obtained Φ_L for higher ρ values (Table S8). In addition,

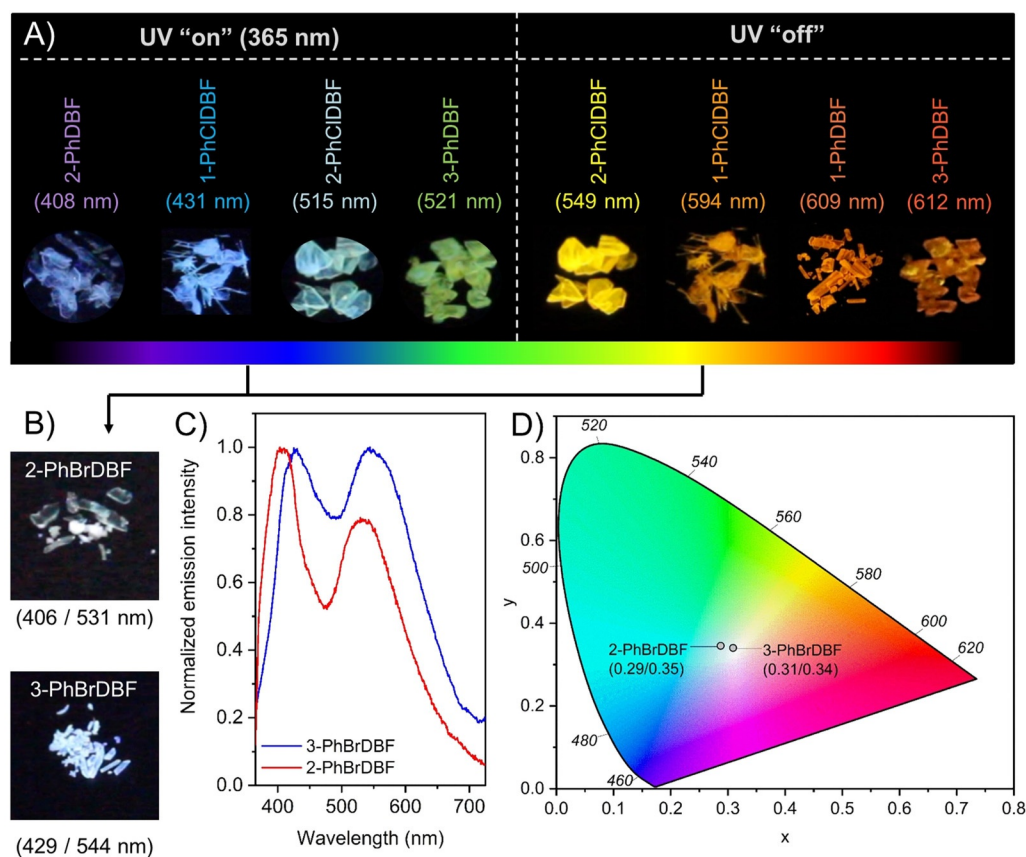


Figure 2. A) Photographs of selected compounds under 365 nm-light excitation and immediately after switching off the UV-light source (0–40 ms due to the experimental setup, see Supporting Information for details). In each case, the wavelength of the emission maximum is detailed in parentheses; the corresponding wavelengths of the afterglow are given after 50 ms delay ($\lambda_{\text{ex}} = 376,7$ nm). B) Photographs of 2-PhBrDBF and 3-PhBrDBF showing white light emission ($\lambda_{\text{ex}} = 365$ nm). The wavelengths correspond to the maxima of the two emission shoulders ($\lambda_{\text{ex}} = 350$ nm). C) Emission spectra of 2-PhBrDBF and 3-PhBrDBF at 350 nm excitation. D) CIE diagram of 2-PhBrDBF and 3-PhBrDBF at 350 nm excitation.

a similar correlation between Φ_L and ρ were also found for the other isomers, with only one exception, namely 3-PhIDBF (Table S8). To clarify, despite the higher ρ , 3-PhIDBF displays low Φ_L (4%) if compared with its predecessor 1-PhIDBF (8%). This is caused by the heavy atom effect, where the presence of iodine can induce non-radiative decays in 3-PhIDBF, based on an extra I...I (3.3%) interaction (Table S8). Additionally, the significantly increased SOC values for the iodinated compounds enables a fast ISC channel from T_1 to S_0 , which competes with room temperature-phosphorescence.^[32] It is worth to mention that while non-covalent interactions are also an important contributor to observe phosphorescence, they are not the key factor. In this regard, we found an interesting correlation between the long lifetime and chromophore (DBF) stacking, which has been already described for carbazole moieties in literature.^[13]

As observed, those isomers featuring the longest lifetime (2-PhCIDBF and 2-PhBrDBF) also exhibit significant DBF-DBF interactions in a perpendicular T-shaped fashion (Figure 3). Interestingly, this kind of DBF-DBF stacking was not observed for the isomers with shorter lifetimes, such as 1-PhCIDBF and 1-PhBrDBF (Figure 3 and S134–S139). With the purpose to identify the role of the DBF-DBF stacking and its influence on the photophysical parameters, natural tran-

sition orbital (NTO) calculations were performed (Figures S132–S133). Notably, NTO calculations showed that the DBF moiety participates on the lowest excited triplet state (T_1), which plays a key role on the origin of the observed phosphorescence. Hence, the DBF-DBF interactions have a direct influence on the photoexcited states. This feature might have two consequences beneficial for ultra-long phosphorescence lifetimes: (1) Short intramolecular non-covalent bonds between neighboring DBF units efficiently suppress molecular vibrations in the crystal and/or (2) strong DBF-DBF stacking stabilizes the photo-induced triplet excitons with charge-transfer character. As shown in Figure 3, two perpendicular DBF-DBF moieties exhibit strong C–H...O interactions in 2-PhCIDBF (2.653 Å) and 2-PhBrDBF (2.665 Å). Such a strong chromophore stacking was only observed for these two isomers, resulting in the ultra-long average lifetimes for 2-PhCIDBF (150 ms) and 2-PhBrDBF (164 ms), which are considerably above the other analogues. In order to gain a deeper understanding of the ground lying role of DBF-DBF and other noncovalent interactions behind the ultra-long phosphorescence, the used crystals were heavily ground and investigated afterwards. Interestingly, absence or significant loss of phosphorescence upon mechanical perturbation infers the importance of DBF-DBF and

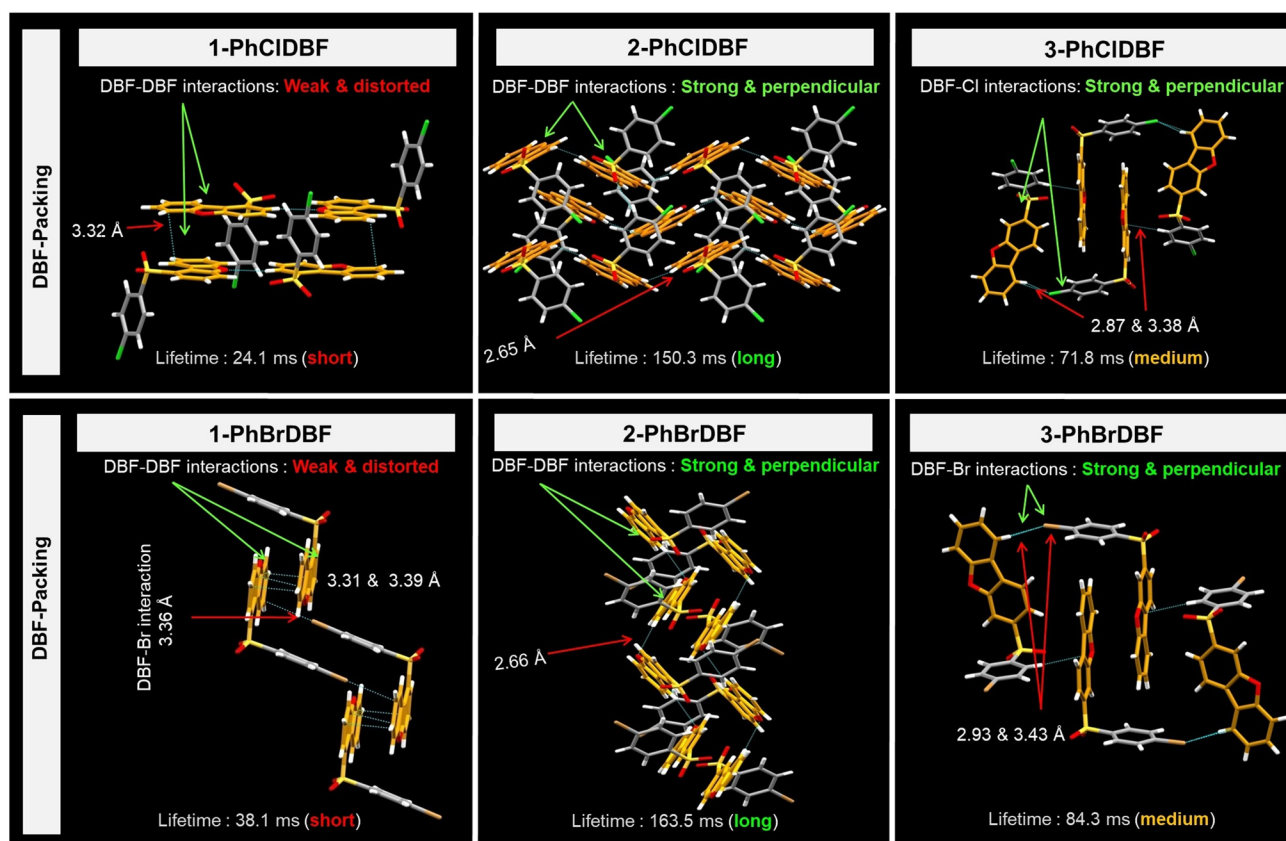


Figure 3. Demonstration of regioisomerism-controlled chromophore stacking in the crystal of the bromo- and chloro-substituted isomers. The isomers that show strong perpendicular DBF-DBF stacking also show longer lifetimes (e.g. 2-PhCIDBF and 2-PhBrDBF). All other interactions have been omitted for clarity.

other noncovalent interactions, which was also evidenced by powder diffraction (PXRD) pattern changes after grinding (Figure S142–S147).

Finally, theoretical calculations based on a two-layer ONIOM model (our own n -layered integrated molecular orbital and molecular mechanics)^[33] extracted from the crystal structure was employed with a combined quantum mechanics/molecular mechanics (QM/MM) method to evaluate the energy level of molecular aggregates in the crystalline state (see Supporting Information for details). The central dimer was chosen as the active QM part (B3LYP/Def2SVP),^[34] while all surrounding molecules were considered as MM part using a universal force field (UFF) (Figure S140). Effective S_1 to T_n transition channels were considered based on a maximal single-triplet energy gap threshold, that is, $|\Delta E_{ST}| \leq 0.3$ eV.^[35] Herein, spin orbit coupling (SOC) constants were not considered to avoid complications with high SOC values above this threshold or low SOC values below the considered $|\Delta E_{ST}|$, respectively (see Note S1 in the supporting information). The most important observation from the QM/MM calculations was the appearance of a higher density of triplet states for the dimers within the crystal, when compared to the monomeric species (Figure 4, Figure S141). For example, the monomer of the 2-PhBrDBF isomer has only three efficient ISC channels (efficient channel considered for $|\Delta E_{ST}| \leq 0.3$ eV).^[35] How-

ever, the number of available ISC-active channels rises to four in the case of the dimer within the crystal. Similarly, the 2-PhCIDBF isomer exhibits three and six main ISC-active pathways for the monomer and the dimer in the crystalline state, respectively. Increasing the number of the ISC-relevant triplet states was also monitored for other isomers (Figure 4 and S141). As shown, the increase of plausible ISC channels in the aggregated form facilitates the generation of triplet excitons. The relevant higher density of triplet states can be accompanied by longer lifetimes due to chromophore stacking (see above), which will finally lead to phosphorescence at room temperature. As expected, when the different isomers are dissolved in organic solvents, the formation and stabilization of triplet excitons due to chromophore stacking is absent and hence no phosphorescence is observed. As envisioned, the calculated excited singlet and triplet state energies vary for the different regioisomers (Figure 4, Figure S141), which is the main reason for the different emission colors under steady-state UV excitation and for the observed phosphorescent afterglow. These rational design criteria using tunable regioisomers yields ultralong lifetimes along with a full spectrum of emission colors including white light, which can be useful for diverse technologies.

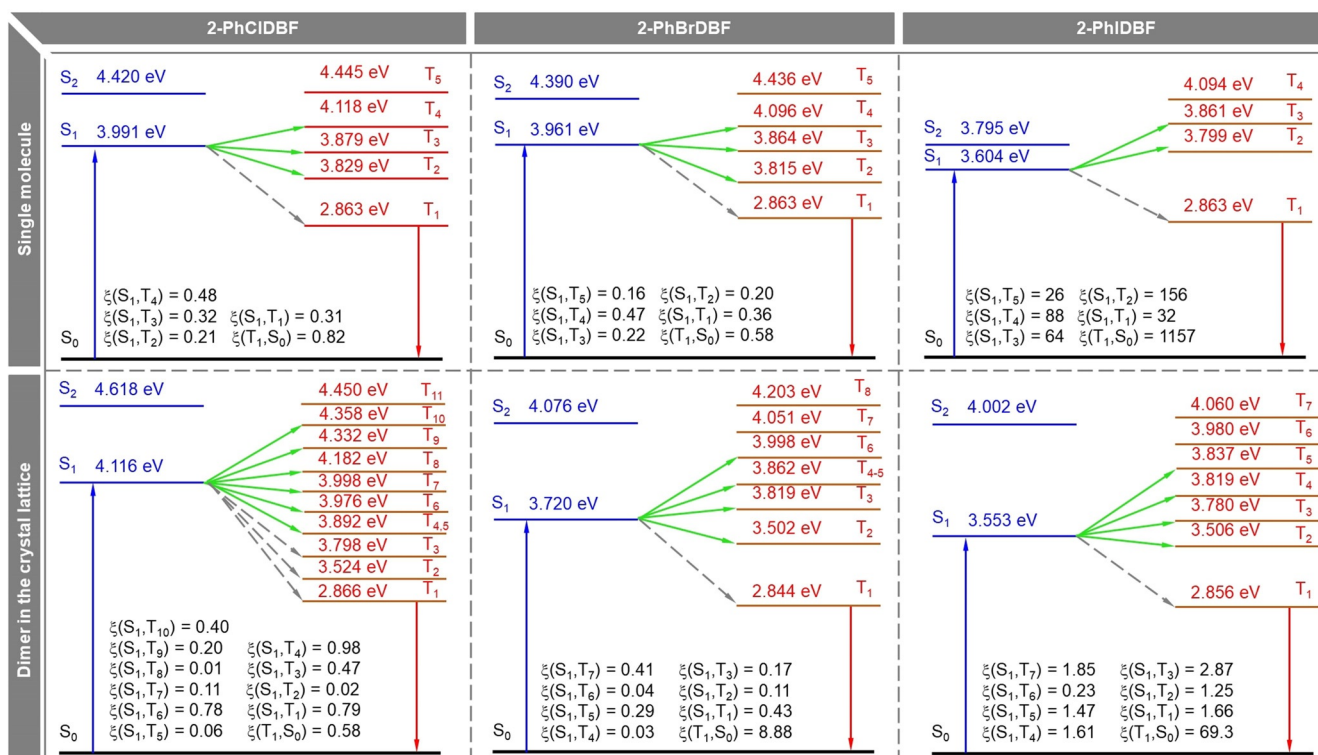


Figure 4. Calculated ISC channels for monomer and the dimer of 2-PhCIDBF, 2-PhBrDBF and 2-PhIDBF isomers in a crystalline environment obtained from two-layer ONIOM calculations at the quantum mechanics/molecular mechanics (QM/MM) level. Solid green lines indicate effective ISC channels within energy level between S₁ and T₁ that is, $|\Delta E_{ST}| \leq 0.3$ eV. Calculated SOC values (ξ , in cm⁻¹) were provided in each case.

Conclusion

Twelve regioisomers of benzenesulfone containing DBF have been synthesized and characterized. Notably, their photophysical properties showed that, based on the accompanying halogen and the type of isomer used, the emission wavelength can be fine-tuned to generate different colors, and even white light from a single compound can be generated. In addition, ultra-long lifetimes were obtained for all the evaluated materials, depending on the halogen and on the type of regioisomer. We found that chromophore stacking assisting the stabilization of triplet excitons along with the enhanced intersystem crossing (ISC) in the crystalline state plays the main role towards long-lived phosphorescence at room temperature. We envision that this work will constitute a straightforward strategy to realize a fully tunable range of visible colors (even white light). Various applications could be addressed, based on this notable class of regioisomerism-controlled dual emitters with long phosphorescent afterglow (of the order of hundreds of ms) and remarkably high photoluminescence quantum yields (up to 22%). The results and their rationalization provide a suitable platform for the advancement towards the next generation of sustainable photoactive materials without employing expensive or scarce elements.

Acknowledgements

We are indebted to the anonymous reviewers for their constructive advice for the improvement of the work. J.V. and B.R. acknowledge the Center for Nanointegration Duisburg-Essen (CENIDE) and the University of Duisburg-Essen for financial support. I.M. gratefully acknowledges the post-doctoral fellowship from the Alexander von Humboldt Foundation. We additionally acknowledge Jan Balszuweit, Kristy Lam, and Robin Meya for experimental assistance. This work was supported by the DFG/Land NRW (INST 211/915-1 FUGG: „Integrated confocal luminescence spectrometer with spatiotemporal resolution and multiphoton excitation“, C.A.S.). This project was additionally financially supported by the Research Grants Council of Hong Kong (16306620, N-HKUST609/19, C6014-20W, and C6009-17G, funding to B.Z.T.), and the Innovation and Technology Commission (ITC-CNERC14SC01, funding to B.Z.T.). Open Access funding enabled and organized by Projekt DEAL.

Conflict of Interest

The authors declare no conflict of interest.

Stichwörter: dibenzofuran · luminophores · phosphorescence · ultralong lifetimes · white light emission

- [1] B. Testa, G. Vistoli, A. Pedretti, *Eur. J. Pharm. Sci.* **2016**, *88*, 101–123.
- [2] A. M. Evans, *Clin. Rheumatol.* **2001**, *20*, 9–14.
- [3] a) N. Chhabra, M. L. Aseri, D. Padmanabhan, *Int. J. Appl. Basic. Med. Res.* **2013**, *3*, 16–18; b) C. Poriol, J. Rault-Berthelot, *Acc. Chem. Res.* **2018**, *51*, 1818–1830; c) S. A. Sharber, S. W. Thomas, *Chem. Mater.* **2020**, *32*, 5785–5801.
- [4] a) M. K. Etherington, F. Franchello, J. Gibson, T. Northey, J. Santos, J. S. Ward, H. F. Higginbotham, P. Data, A. Kurowska, P. L. Dos Santos, D. R. Graves, A. S. Batsanov, F. B. Dias, M. R. Bryce, T. J. Penfold, A. P. Monkman, *Nat. Commun.* **2017**, *8*, 14987; b) C. Chen, Z. Chi, K. C. Chong, A. S. Batsanov, Z. Yang, Z. Mao, Z. Yang, B. Liu, *Nat. Mater.* **2021**, *20*, 175–180; c) Y. Xiong, Z. Zhao, W. Zhao, H. Ma, Q. Peng, Z. He, X. Zhang, Y. Chen, X. He, J. W. Y. Lam, B. Z. Tang, *Angew. Chem. Int. Ed.* **2018**, *57*, 7997–8001; *Angew. Chem.* **2018**, *130*, 8129–8133; d) A. M. Philip, M. Gudem, E. Sebastian, M. Hariharan, *J. Phys. Chem. A* **2019**, *123*, 6105–6112.
- [5] a) S. M. A. Fatemina, Z. Mao, S. Xu, Z. Yang, Z. Chi, B. Liu, *Angew. Chem. Int. Ed.* **2017**, *56*, 12160–12164; *Angew. Chem.* **2017**, *129*, 12328–12332; b) Y. Wang, H. Gao, J. Yang, M. Fang, D. Ding, B. Z. Tang, Z. Li, *Adv. Mater.* **2021**, *33*, 2007811; c) S. M. Parke, E. Hupf, G. K. Matharu, I. de Aguiar, L. Xu, H. Yu, M. P. Boone, G. L. C. de Souza, R. McDonald, M. J. Ferguson, G. He, A. Brown, E. Rivard, *Angew. Chem. Int. Ed.* **2018**, *57*, 14841–14846; *Angew. Chem.* **2018**, *130*, 15057–15062; d) H. Ma, Q. Peng, Z. An, W. Huang, Z. Shuai, *J. Am. Chem. Soc.* **2019**, *141*, 1010–1015; e) W. J. Zhao, Z. K. He, B. Z. Tang, *Nat. Rev. Mater.* **2020**, *5*, 869–885.
- [6] N. Yanai, N. Kimizuka, *Acc. Chem. Res.* **2017**, *50*, 2487–2495.
- [7] S. Koseki, N. Matsunaga, T. Asada, M. W. Schmidt, M. S. Gordon, *J. Phys. Chem. A* **2019**, *123*, 2325–2339.
- [8] a) M. Jin, T. S. Chung, T. Seki, H. Ito, M. A. Garcia-Garibay, *J. Am. Chem. Soc.* **2017**, *139*, 18115–18121; b) Q. Zhao, F. Li, C. Huang, *Chem. Soc. Rev.* **2010**, *39*, 3007–3030.
- [9] a) L. Gu, X. Wang, M. Singh, H. Shi, H. Ma, Z. An, W. Huang, *J. Phys. Chem. Lett.* **2020**, *11*, 6191–6200; b) S. Mukherjee, P. Thilagar, *Chem. Commun.* **2015**, *51*, 10988–11003.
- [10] a) W. J. Zhao, Z. K. He, J. W. Y. Lam, Q. Peng, H. L. Ma, Z. G. Shuai, G. X. Bai, J. H. Hao, B. Z. Tang, *Chem* **2016**, *1*, 592–602; b) Kenry, C. Chen, B. Liu, *Nat. Commun.* **2019**, *10*, 2111.
- [11] a) T. Itoh, *Chem. Rev.* **2012**, *112*, 4541–4568; b) G. Baryshnikov, B. Minaev, H. Agren, *Chem. Rev.* **2017**, *117*, 6500–6537.
- [12] a) M. Hayduk, S. Riebe, J. Voskuhl, *Chem. Eur. J.* **2018**, *24*, 12221–12230; b) S. M. Parke, E. Rivard, *Isr. J. Chem.* **2018**, *58*, 915–926.
- [13] N. Gan, X. Wang, H. Ma, A. Lv, H. Wang, Q. Wang, M. Gu, S. Cai, Y. Zhang, L. Fu, M. Zhang, C. Dong, W. Yao, H. Shi, Z. An, W. Huang, *Angew. Chem. Int. Ed.* **2019**, *58*, 14140–14145; *Angew. Chem.* **2019**, *131*, 14278–14283.
- [14] Y. Su, S. Z. F. Phua, Y. Li, X. Zhou, D. Jana, G. Liu, W. Q. Lim, W. K. Ong, C. Yang, Y. Zhao, *Sci. Adv.* **2018**, *4*, eaas9732.
- [15] J. Zhang, S. Xu, Z. Wang, P. Xue, W. Wang, L. Zhang, Y. Shi, W. Huang, R. Chen, *Angew. Chem. Int. Ed.* **2021**, *60*, 17094–17101; *Angew. Chem.* **2021**, *133*, 17231–17238.
- [16] H. Shi, L. Zou, K. Huang, H. Wang, C. Sun, S. Wang, H. Ma, Y. He, J. Wang, H. Yu, W. Yao, Z. An, Q. Zhao, W. Huang, *ACS Appl. Mater. Interfaces* **2019**, *11*, 18103–18110.
- [17] a) H. Sun, S. Liu, W. Lin, K. Y. Zhang, W. Lv, X. Huang, F. Huo, H. Yang, G. Jenkins, Q. Zhao, W. Huang, *Nat. Commun.* **2014**, *5*, 3601; b) H. Xiang, J. Cheng, X. Ma, X. Zhou, J. J. Chruma, *Chem. Soc. Rev.* **2013**, *42*, 6128–6185.
- [18] J. Chen, X. Chen, Y. Liu, Y. Li, J. Zhao, Z. Yang, Y. Zhang, Z. Chi, *Chem. Sci.* **2021**, *12*, 9201–9206.
- [19] S. L. Sonawane, S. K. Asha, *J. Phys. Chem. B* **2014**, *118*, 9467–9475.
- [20] a) Z. He, W. Zhao, J. W. Y. Lam, Q. Peng, H. Ma, G. Liang, Z. Shuai, B. Z. Tang, *Nat. Commun.* **2017**, *8*, 416; b) B. Roy, M. C. Reddy, G. P. Jose, F. C. Niemeyer, J. Voskuhl, P. Hazra, *J. Phys. Chem. Lett.* **2021**, *12*, 1162–1168.
- [21] X. Q. Bi, Y. G. Shi, T. Peng, S. W. Yue, F. Wang, L. Y. Zheng, Q. E. Cao, *Adv. Funct. Mater.* **2021**, *31*, 2101312.
- [22] a) B. Xu, H. Wu, J. Chen, Z. Yang, Z. Yang, Y. C. Wu, Y. Zhang, C. Jin, P. Y. Lu, Z. Chi, S. Liu, J. Xu, M. Aldred, *Chem. Sci.* **2017**, *8*, 1909–1914; b) Y. T. Wen, H. C. Liu, S. T. Zhang, J. G. Cao, J. B. De, B. Yang, *Adv. Opt. Mater.* **2020**, *8*, 1901995; c) H. Bhatia, D. Ray, *J. Phys. Chem. C* **2019**, *123*, 22104–22113; d) J. A. Li, J. Zhou, Z. Mao, Z. Xie, Z. Yang, B. Xu, C. Liu, X. Chen, D. Ren, H. Pan, G. Shi, Y. Zhang, Z. Chi, *Angew. Chem. Int. Ed.* **2018**, *57*, 6449–6453; *Angew. Chem.* **2018**, *130*, 6559–6563.
- [23] a) J. Hu, Q. Li, X. Wang, S. Shao, L. Wang, X. Jing, F. Wang, *Angew. Chem. Int. Ed.* **2019**, *58*, 8405–8409; *Angew. Chem.* **2019**, *131*, 8493–8497; b) H. W. Mo, Y. Tsuchiya, Y. Geng, T. Sagawa, C. Kikuchi, H. Nakanotani, F. Ito, C. Adachi, *Adv. Funct. Mater.* **2016**, *26*, 6703–6710.
- [24] a) Z. Q. Li, Z. L. Gong, J. Y. Shao, J. Yao, Y. W. Zhong, *Angew. Chem. Int. Ed.* **2021**, *60*, 14595–14600; *Angew. Chem.* **2021**, *133*, 14716–14721; b) C. Liu, H. Bai, B. He, X. He, J. Zhang, C. Chen, Y. Qiu, R. Hu, F. Zhao, Y. Zhang, W. He, J. H. C. Chau, S. Chen, J. W. Y. Lam, B. Z. Tang, *Angew. Chem. Int. Ed.* **2021**, *60*, 12424–12430; *Angew. Chem.* **2021**, *133*, 12532–12538; c) K. Jiang, S. Sun, L. Zhang, Y. Lu, A. Wu, C. Cai, H. Lin, *Angew. Chem. Int. Ed.* **2015**, *54*, 5360–5363; *Angew. Chem.* **2015**, *127*, 5450–5453.
- [25] B. Liégault, D. Lee, M. P. Huestis, D. R. Stuart, K. Fagnou, *J. Org. Chem.* **2008**, *73*, 5022–5028.
- [26] a) K. L. Marsi, S. H. Wilen, *J. Chem. Educ.* **1963**, *40*, 214–215; b) N. O. Calloway, *Chem. Rev.* **1935**, *17*, 327–392.
- [27] M. Baba, *J. Phys. Chem. A* **2011**, *115*, 9514–9519.
- [28] Deposition Numbers 2094631, 2094632, 2094633, 2094634, 2094635, 2096541, 2096542, 2096543, 2096544, 2096545, 2096546 and 2096564 contain the supplementary crystallographic data for this paper. These data are provided free of charge by the joint Cambridge Crystallographic Data Centre and Fachinformationszentrum Karlsruhe Access Structures service www.ccdc.cam.ac.uk/structures.
- [29] T. Zhang, X. Wang, Z. An, Z. Fang, Y. Zhang, W. Z. Yuan, *ChemPhysChem* **2018**, *19*, 2389–2396.
- [30] P. R. Spackman, M. J. Turner, J. J. McKinnon, S. K. Wolff, D. J. Grimwood, D. Jayatilaka, M. A. Spackman, *J. Appl. Crystallogr.* **2021**, *54*, 1006–1011.
- [31] B. Roy, M. C. Reddy, P. Hazra, *Chem. Sci.* **2018**, *9*, 3592–3606.
- [32] A. Lv, W. Ye, X. Jiang, N. Gan, H. Shi, W. Yao, H. Ma, Z. An, W. Huang, *J. Phys. Chem. Lett.* **2019**, *10*, 1037–1042.
- [33] T. Vreven, K. Morokuma in *Annual Reports in Computational Chemistry, Vol. 2* (Ed.: D. C. Spellmeyer), Elsevier, Amsterdam, **2006**, pp. 35–51.
- [34] a) F. Weigend, R. Ahlrichs, *Phys. Chem. Chem. Phys.* **2005**, *7*, 3297–3305; b) A. D. Becke, *J. Chem. Phys.* **1993**, *98*, 5648–5652.
- [35] a) Z. Yang, Z. Mao, X. Zhang, D. Ou, Y. Mu, Y. Zhang, C. Zhao, S. Liu, Z. Chi, J. Xu, Y. C. Wu, P. Y. Lu, A. Lien, M. R. Bryce, *Angew. Chem. Int. Ed.* **2016**, *55*, 2181–2185; *Angew. Chem.* **2016**, *128*, 2221–2225; b) J. Yang, Z. Ren, Z. Xie, Y. Liu, C. Wang, Y. Xie, Q. Peng, B. Xu, W. Tian, F. Zhang, Z. Chi, Q. Li, Z. Li, *Angew. Chem. Int. Ed.* **2017**, *56*, 880–884; *Angew. Chem.* **2017**, *129*, 898–902.

Manuskript erhalten: 31. August 2021

Veränderte Fassung erhalten: 12. Oktober 2021

Akzeptierte Fassung online: 25. Oktober 2021

Endgültige Fassung online: 7. Dezember 2021